Power-Cable Temperature Reconstruction from Electromagnetic Reflectometry Data

Guus Doldersum

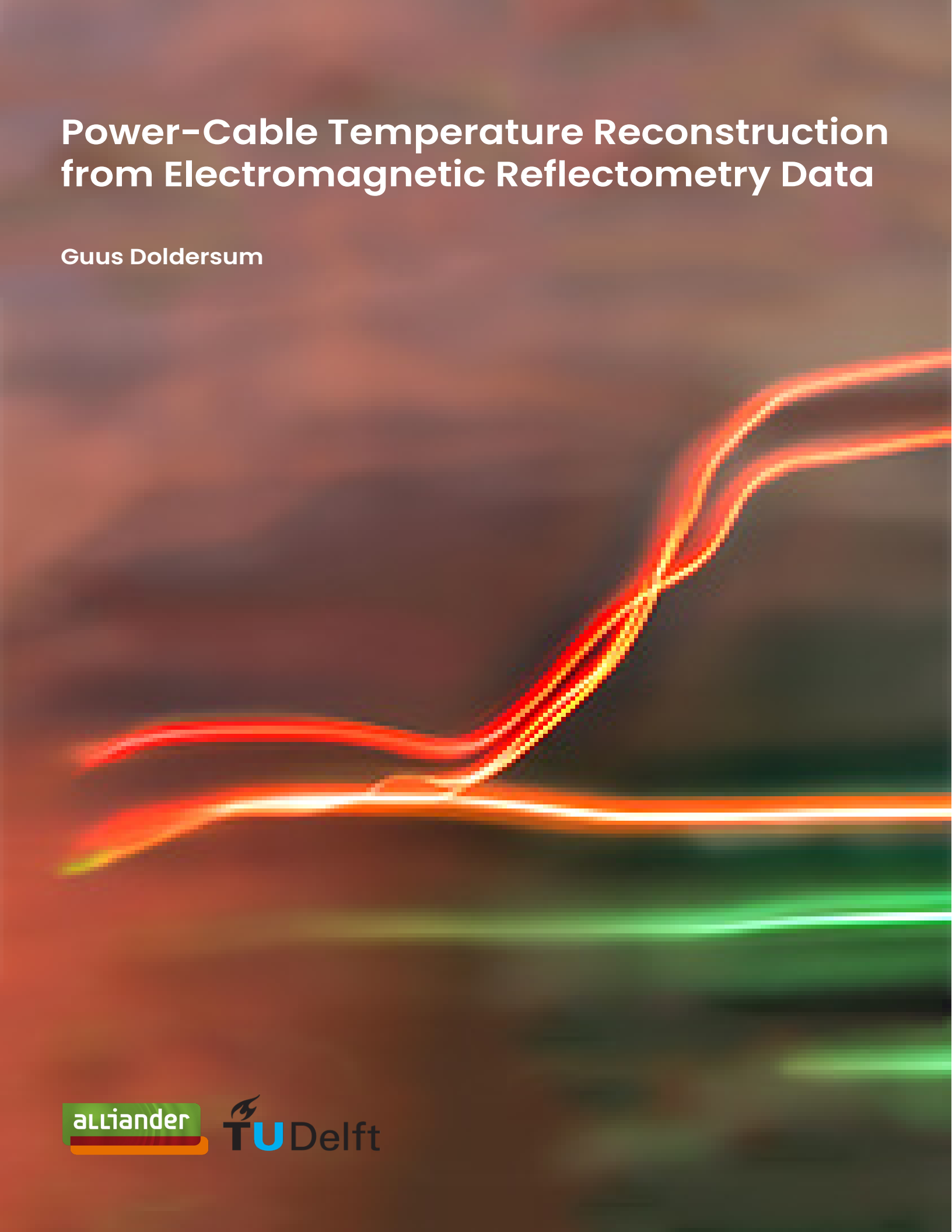

Power-Cable Temperature Reconstruction from Electromagnetic Reflectometry Data

by

Guus Doldersum

Student number: 5403685
Project duration: April 22, 2024 – June 22, 2024
Thesis committee: Dr. ir. N.V. Budko, TU Delft, supervisor
Dr. ir. N. Parolya, TU Delft

Acknowledgement

First of all I would like to thank my professor Neil Budko. Without Neil's guidance this research would not have been possible. He was crucial for the mathematical model and theoretical insight in the encountered problems. But also his enthusiasm, motivational words and great communication were highly encouraging and essential for the completion of the project.

I would to thank Alliander B.V. for the opportunity to carry out my bachelor thesis with them. To be able to contribute a small part in a very interesting and important research project was a valuable addition to me. I enjoyed the days I spent at Alliander in the Arnhem office. It was motivating to work together with the colleagues at Alliander and I enjoyed the nice atmosphere, open and friendly culture at Alliander.

I'd like to thank the colleagues from Alliander who were involved in some way or another in my project. My appreciation goes to all of them. I would especially like to mention Sander Rieken, Ferran Faura Iglesias and Niels de Visser. I still remember my first day at the office clearly when each of you took the time to learn me the ropes. I wish you all the best and good progress with the continuation of the project.

Finally, I would like to thank my family and friends for their support during this hectic period. My parents were always there to listen when I needed to talk about the challenges I faced, and my friends provided much-needed distraction when I needed a break. Your support has been invaluable.

Abstract

This paper addresses the challenge of accurately monitoring power cable temperatures, which is crucial for the reliability and efficiency of electrical power systems during the energy transition. Overheating of power cables can lead to insulation failure and reduced lifespan, making precise temperature monitoring essential.

Recent research by Alliander has explored the use of electromagnetic reflectometry for the reconstruction of power cable temperatures by analyzing the propagation time of pulsed electromagnetic signals within the cable. This study aims to improve upon this by directly reconstructing the electromagnetic parameters of the power cable and understanding their temperature dependence through a controlled experiment.

Key steps include:

- Cable Modeling: Using the Telegrapher's equations to describe voltage and current distributions in the time and frequency domains.
- Data Transformation: Converting these equations into integral equations and discretizing them to define an inverse scattering problem.
- Experimental Validation: Using synthetic data and data from a temperature-controlled experiment by Alliander to test and refine the reconstruction method

The study reconstructs the electrical parameters of the cable and attempts to find a relation between the parameters and the cable temperature. This method attempts a more accurate temperature monitoring system, enhancing the safety and efficiency of power grids

Contents

Chapter 1

Introduction

The energy transition is one of the most significant challenges of the coming decades. A key aspect of this transition involves enhancing the reliability and efficiency of the power grid. Accurate monitoring of power cable temperatures is essential for maintaining these qualities in electrical power systems. While maximizing the performance of power cables is important, overheating can lead to insulation failure and a reduced cable lifespan. Therefore, developing reliable methods to measure and reconstruct power cable temperatures is essential for ensuring the safe and efficient operation of electrical networks.

Recent research initiated by Alliander has explored the relationship between the power-cable temperatures and the propagation time of a pulsed electromagnetic signal inside the cable. The research by Wouters et al. [1] demonstrated the potential of electromagnetic reflectometry for temperature reconstruction. However, it was noted that the currently achievable accuracy in the reconstruction of the cable parameters may be insufficient for a sufficiently precise temperature reconstruction.

The present study aims to analyze the properties of power cables and the behavior of their parameters as the cable-temperature varies. We use the data from an experiment conducted by Alliander, where the relationship between the cable-temperature and the propagation time was investigated for a single piece of isolated cable. Our approach is to utilize the reflectometry data to directly reconstruct the constitutive parameters of the power cable by solving an inverse scattering problem, rather than approximately measuring the EM pulse propagation time. Then, by finding the polynomial fit for the temperature dependence of the reconstructed parameters in the controlled-temperature experiment, we should be able to deduce the temperature in any realistic conditions.

Our approach involves several key steps. First, we will describe a power cable using widely accepted partial differential equations (PDE's) in the time and frequency domains, which describe the current and voltage distributions along a power cable. We will then transform these PDE's into integral equations. Next, we will discretize the integral equations and define the inverse scattering problem. Finally, we use synthetic data and the experimental data from Alliander to reconstruct the parameters of the power cable and to fit the temperature-dependence polynomial.

This innovative approach aims to improve the accuracy of power cable temperature monitoring, contributing to the overall reliability and efficiency of electrical power systems in the context of the energy transition.

Chapter 2

Frequency-domain model of reflectometry data

In this Chapter we use the single-conductor transmission line as a model of a power cable. Multi-conductor cores result in more complicated models. However, the difference between the latter sophisticated model and the simple single-conductor model can be subsumed into the effective transmission-line parameters. The propagation of the electromagnetic wave along a transmission line is described by the Telegrapher's equations. First we formulate these equations in the time domain, then we transform the problem to the frequency domain with the help of the Fourier transform and derive the second-order differential equation for the complex voltage amplitude. After that, we introduce the scattering formalism and apply the Green's function approach to transform the problem into the integral equation.

2.1 Telegrapher's equations in time domain

The voltage $U(x,t)$ and the current $I(x,t)$ along the transmission line are the functions of the time t and the position x along the cable. A power cable is characterized by the (effective) resistance R (of the conductor) and the inductance L in series and the capacitance C and the conductance G (of the propagating medium) in parallel. The resistance and conductance contribute to the losses in a transmission line. The effective constitutive parameters of the cable may depend on the temperature T and the location x.

The propagation of the electromagnetic wave along the transmission line is governed by the following coupled system of partial differential equations involving the voltage and the current induced by the wave:

$$\begin{aligned} -\frac{\partial U}{\partial x} &= RI + L\frac{\partial I}{\partial t} + f, \\ -\frac{\partial I}{\partial x} &= GU + C\frac{\partial U}{\partial t}, \end{aligned} \tag{2.1}$$

where $f(x,t)$ is the source function. We describe a cable of a finite length, stretching between a and b along the x-axis, by defining R, G, L, C as follows:

$$R(x), G(x), L(x), C(x) = \begin{cases} R(x,T), G(x,T), L(x,T), C(x,T), & x \in [a,b] \\ 0, 0, \mu_0, \epsilon_0, & x \notin [a,b] \end{cases} \tag{2.2}$$

2.2 Telegrapher's equations in frequency domain

We use the Fourier transform to convert the differential equations from the time domain into the frequency domain. The following properties of Fourier transform are employed: [8]

$$\begin{aligned}\hat{f}(x,\omega) &= \int_{\mathbb{R}} f(x,t)e^{-j\omega t}\,\mathrm{d}t \\ f(x,t) &= \frac{1}{2\pi}\int_{\mathbb{R}} \hat{f}(x,\omega)e^{j\omega t}\,\mathrm{d}t \\ j\omega\hat{f}(x,\omega) &= \int_{\mathbb{R}} \frac{\partial}{\partial t} f(x,t)e^{-j\omega t}\,\mathrm{d}t,\end{aligned}$$

where j denotes the imaginary unit. The resulting system of ordinary differential equations (ODE's) describing the transmission line in the frequency domain is:

$$\begin{aligned}\frac{d\hat{U}}{dx} &= -(R+j\omega L)I + \hat{f}, \\ \frac{d\hat{I}}{dx} &= -(G+j\omega C)\hat{U}\end{aligned} \tag{2.3}$$

If we differentiate the first equation one more time and substitute there the expression for $\frac{d\hat{I}}{dx}$ obtained from the second equation we arrive at the second-order ODE for the frequency-domain voltage:

$$\frac{d^2\hat{U}}{dx^2} - \gamma^2\hat{U} = \frac{d\hat{f}}{dx}, \tag{2.4}$$

where $\gamma(x,\omega)$ is the cable propagation constant (related to the wavenumber):

$$\gamma^2(x,\omega) = (R+j\omega L)(G+j\omega C) = \alpha + j\beta \tag{2.5}$$

$$\gamma_0^2(\omega) = -\omega^2\mu_0\epsilon_0. \tag{2.6}$$

The real and imaginary parts, α and β, of the squared propagation constant are called the attenuation and phase constants, respectively, and $\omega\sqrt{\epsilon_0\mu_0}$ is the vacuum wavenumber.

2.3 Scattering formalism

In the scattering formalism, the total voltage inside the cable is decomposed into the sum of the incident and scattered voltages:

- $\hat{u}$: Total voltage ($\hat{U}$) produced by the source $\hat{f}$ in the actual transmission line with the wavenumber $\gamma(x,\omega)$.
- $\hat{u}^{\mathrm{in}}$: Incident voltage. This is the voltage profile that the same source $\hat{f}$ would create in the transmission line with the wavenumber $\gamma_0(\omega)$.
- $\hat{u}^{\mathrm{sc}} = \hat{u} - \hat{u}^{\mathrm{in}}$: Scattered voltage.

The incident and the total voltages satisfy the following equations:

$$\frac{d^2\hat{u}^{\mathrm{in}}}{dx^2} - \gamma_0^2\hat{u}^{\mathrm{in}} = \frac{d\hat{f}}{dx}, \tag{2.7}$$

$$\frac{d^2\hat{u}}{dx^2} - \gamma^2\hat{u} = \frac{d\hat{f}}{dx}. \tag{2.8}$$

It is easy to show that the scattered voltage satisfies:

$$\frac{d^2\hat{u}^{\mathrm{sc}}}{dx^2} - \gamma_0^2\hat{u}^{\mathrm{sc}} = (\gamma^2 - \gamma_0^2)\hat{u}. \tag{2.9}$$

Obviously, the source of the scattered voltage is the so-called contrast source $(\gamma^2 - \gamma_0^2)\hat{u}$, which differs from zero only within the finite cable, where $\gamma^2(x,\omega) - \gamma_0^2(\omega) \neq 0$.

2.4 Integral equations

In this section we rewrite the differential equations Equation (2.7) and Equation (2.9) as integral equations.

Definition 2.4.1 (Green's function [9]) *The frequency-domain Green's function $g(x-x',\omega)$ is defined as the solution of the following equation*

$$\frac{d^2g}{d^2x^2} - \gamma_0^2 g = \delta(x-x'), \tag{2.10}$$

where $\delta(x)$ denotes the generalized Dirac's delta function.

To obtain the explicit expression for the vacuum Green's function we use the spatial Fourier transform with the following properties:

$$\begin{aligned}
\mathcal{F}[g(x,\omega)] = \tilde{g}(k,\omega) &= \int_{\mathbb{R}} g(x,\omega)e^{-jkx}\mathrm{d}x \\
\mathcal{F}\left[\frac{d^2g}{dx^2}\right] &= -k^2\tilde{g}(k,\omega) \\
\mathcal{F}[\delta(x)] &= 1
\end{aligned}$$

Applying this to the differential equation that defines the Green's function, we obtain:

$$-k^2\tilde{g} - \gamma_0^2\tilde{g} = 1$$

Solving the resulting algebraic equation we arrive at the expression for the k-domain Green's function:

$$\tilde{g}(k,\omega) = -\frac{1}{(k^2+\gamma_0^2)} \tag{2.11}$$

The inverse Fourier transform of $\hat{g}(k,\omega)$ gives:

$$\begin{aligned}
g(x,\omega) &= \frac{1}{2\pi}\int_{\mathbb{R}} \tilde{g}(x,\omega)e^{jkx}\mathrm{d}k \\
g(x,\omega) &= -\frac{1}{2\pi}\int_{\mathbb{R}} \frac{1}{k^2+\gamma_0^2}e^{jkx}\mathrm{d}k \\
g(x,\omega) &= -\frac{1}{2\gamma_0 2\pi}\int_{\mathbb{R}} \frac{2\gamma_0}{k^2+\gamma_0^2}e^{jkx}\mathrm{d}k \\
g(x,\omega) &= -\frac{1}{2\gamma_0}e^{-\gamma_0|x|}\mathrm{d}k \\
g(x-x',\omega) &= -\frac{e^{-\gamma_0|x-x'|}}{2\gamma_0}
\end{aligned} \tag{2.12}$$

Theorem 2.4.1 (Green's Theorem) *Let $g(x,\omega)$ be the Green's function satisfying the equation (2.10). Then, for any $f(x,\omega) \in C(a,b)$, such that $f(x,\omega) = 0$ for $x \notin [a,b]$, the solution of the equation*

$$\frac{d^2u}{dx^2} - \gamma_0^2 u = f$$

can be obtained as

$$u(x) = \int_a^b g(x-x',\omega)f(x',\omega)dx'.$$

Applying Theorem 2.4.1 to Equation (2.9), we obtain the integral relation

$$\hat{u}^{\mathrm{sc}}(x,\omega) = \int_a^b g(x-x',\omega)[\gamma^2(x',\omega) - \gamma_0^2(\omega)]\hat{u}(x',\omega)\mathrm{d}x', \tag{2.13}$$

which describes the scattered voltage at any $x \in \mathbb{R}$, including the point x_{r}, where it is measured in a reflectometry experiment. Using the definition $\hat{u}^{\mathrm{sc}} = \hat{u} - \hat{u}^{\mathrm{in}}$, we arrive at the following integral equation that describes the total voltage distribution in the cable:

$$\hat{u}(x,\omega) - \int_a^b g(x-x',\omega)[\gamma^2(x',\omega) - \gamma_0^2(\omega)]\hat{u}(x',\omega)\mathrm{d}x' = \hat{u}^{\mathrm{in}}(x,\omega), \quad x \in [a,b]. \tag{2.14}$$

The equations (2.13) and (2.14) fully describe both the *forward* and the *inverse* scattering problems. In the forward problem one assumes that the incident voltage $\hat{u}^{\mathrm{in}}$ and the contrast $\gamma^2 - \gamma_0^2$ are given and finds the total voltage $\hat{u}$ by solving (2.14). In the inverse problem one measures the total voltage at some location x_{r}, sometimes at the boundary of the interval $[a,b]$, and uses the equation (2.13) to find the contrast. Since the total voltage at all other points in $[a,b]$ is not known, it is also an unknown in the inverse problem. Therefore, the complete formulation of the inverse problem usually includes both the *data* equation (2.13) and the *object* equation (2.14).

2.5 Decomposition of the contrast function

The contrast function $\gamma^2 - \gamma_0^2$ depends on four (effective) constitutive parameters of the power cable R, G, L and C and the angular frequency ω. While the constitutive parameters may depend on the temperature T of the cable in a complicated way, they do not depend on the frequency. This fact may be used to improve the quality of reconstruction of the constitutive parameters by utilizing the multi-frequency scattered voltage data that become available when the cable is interrogated with a broad-band electromagnetic pulse. To make this possible the contrast function must be appropriately decomposed:

$$\gamma^2 - \gamma_0^2 = (R + j\omega L)(G + j\omega C) + \omega^2\epsilon_0\mu_0 = \chi_1 + j\omega\chi_2 + \omega^2\chi_3, \tag{2.15}$$

where

$$\begin{aligned} \chi_1(x) &= RG, \\ \chi_2(x) &= RC + G\mu_0, \\ \chi_3(x) &= \mu_0(\epsilon_0 - C). \end{aligned} \tag{2.16}$$

Above we have made the assumption that the cable is essentially non-magnetic, i.e., $L = \mu_0$. Note that the three components χ_i, $i = 1,2,3$ of the contrast function, uniquely define the three constitutive parameters R, G, and C of the power cable.

With the introduced decomposition of the contrast function, the integral equations (2.13) and (2.14) become:

$$\begin{aligned} \hat{u}(x,\omega) &- \int_a^b g(x-x',\omega)\chi_1(x')\hat{u}(x',\omega)\mathrm{d}x' \\ &- j\omega\int_a^b g(x-x',\omega)\chi_2(x')\hat{u}(x',\omega)\mathrm{d}x' \\ &- \omega^2\int_a^b g(x-x',\omega)\chi_3(x')\hat{u}(x',\omega)\mathrm{d}x' = \hat{u}^{\mathrm{in}}(x,\omega), \quad x \in [a,b]. \end{aligned} \tag{2.17}$$

and

$$\begin{aligned}
&\int_a^b g(x_\mathrm{r}-x',\omega)\chi_1(x')\hat{u}(x',\omega)\mathrm{d}x' \\
&+ j\omega\int_a^b g(x_\mathrm{r}-x',\omega)\chi_2(x')\hat{u}(x',\omega)\mathrm{d}x' \\
&+ \omega^2\int_a^b g(x_\mathrm{r}-x',\omega)\chi_3(x')\hat{u}(x',\omega)\mathrm{d}x' = \hat{u}^{\mathrm{sc}}(x_\mathrm{r}),
\end{aligned} \tag{2.18}$$

where we have explicitly assumed that the scattered voltage is measured at the single location x_r.

Chapter 3

Discretization of forward and inverse scattering problems

In this chapter we discretize the integral equations (2.17) and (2.18) in space and derive the corresponding algebraic equations. We use the mid-point rule to approximate the integrals over x' and the collocation method to discretize the second variable x. Then, we introduce the discrete version of the Green's function for a homogeneous finite cable at a base temperature.

3.1 Mid-point approximation and collocation

Theorem 3.1.1 (Mid-point approximation [7]) *Let $f \in C^2[x_{k-1}, x_k]$, $h_k = x_k - x_{k-1}$, $x_m = (x_{k-1} + x_k)/2$, and $m_2 = \max_{\xi\in[x_{k-1},x_k]} |f''(\xi)|$. Then,*

$$\left| \int_{x_{k-1}}^{x_k} f(x)\, dx - h_k f(x_m) \right| \leq \frac{1}{24} m_2 h_k^3$$

Theorem 3.1.2 (Composite integration rule [7]) *Let $f(x)$ be given for $x \in [a, b]$, and let there be a uniform partition $a = x_0 < x_1 < \cdots < x_n = b$, with $x_k = x_0 + kh$, $k = 0, \ldots, n$, $h = (b - a)/n$.*

Let I_k be the approximation of the integral over $[x_{k-1}, x_k]$, such that

$$\left| I_k - \int_{x_{k-1}}^{x_k} f(x)\, dx \right| \leq c_k h^{p+1}, \quad p \in \mathbb{N}.$$

Then,

$$\left| \sum_{k=1}^{n} I_k - \int_a^b f(x)\, dx \right| \leq c(b - a)h^p$$

where $c = \max_k c_k$.

Consider the partitioning of the interval $[a, b]$ into n sub-intervals of equal size $h = (b-a)/n$ and define the grid of n mid-points $x_i = a + h/2 + (i-1)h$, $i = 1, \ldots, n$. Then, according to the composite mid-point rule, the integrals in (2.17) and (2.18) can be approximated by finite sums up to $\mathcal{O}(h^2)$. Collocating the second variable x in (2.17) on the same grid as x', and neglecting the $\mathcal{O}(h^2)$ approximation errors, we arrive at the following discretized version of the integral

equations:

$$\begin{aligned}\hat{u}(x_k,\omega) - h\sum_{i=1}^{n} g(x_k - x_i,\omega)\chi_1(x_i)\hat{u}(x_i,\omega) \\ - j\omega h\sum_{i=1}^{n} g(x_k - x_i,\omega)\chi_2(x_i)\hat{u}(x_i,\omega) \\ - \omega^2 h\sum_{i=1}^{n} g(x_k - x_i,\omega)\chi_3(x_i)\hat{u}(x_i,\omega) = \hat{u}^{\mathrm{in}}(x_k,\omega), \\ x_k = a + h/2 + (k-1)h, \quad k = 1,\ldots,n.\end{aligned} \tag{3.1}$$

$$\begin{aligned}h\sum_{i=1}^{n} g(x_{\mathrm{r}} - x_i,\omega)\chi_1(x_i)\hat{u}(x_i,\omega) \\ + j\omega h\sum_{i=1}^{n} g(x_{\mathrm{r}} - x_i,\omega)\chi_2(x_i)\hat{u}(x_i,\omega) \\ + \omega^2 h\sum_{i=1}^{n} g(x_{\mathrm{r}} - x_i,\omega)\chi_3(x_i)\hat{u}(x_i,\omega) = \hat{u}^{\mathrm{sc}}(x_{\mathrm{r}}),\end{aligned} \tag{3.2}$$

These algebraic equations can be compactly written as

$$[I - G_\omega X_1 - j\omega G_\omega X_2 - \omega^2 G_\omega X_3]\boldsymbol{u}_\omega = \boldsymbol{u}_\omega^{\mathrm{in}}, \tag{3.3}$$

$$\boldsymbol{r}_\omega^T U_\omega \boldsymbol{x}_1 + j\omega \boldsymbol{r}_\omega^T U_\omega \boldsymbol{x}_2 + \omega^2 \boldsymbol{r}_\omega^T U_\omega \boldsymbol{x}_3 = u_\omega^{\mathrm{sc}}, \tag{3.4}$$

where

- $I \in \mathbb{R}^{n\times n}$ is the identity matrix.
- $G_\omega \in \mathbb{C}^{n\times n}$ is the matrix with the elements $[G_\omega]_{k,i} = hg(x_k - x_i,\omega)$.
- $X_m = \mathrm{diag}(\boldsymbol{x}_m) \in \mathbb{R}^{n\times n}$, $m = 1,2,3$, are the diagonal matrices that contain the vectors $\boldsymbol{x}_m \in \mathbb{R}^n$ with the elements $[\boldsymbol{x}_m]_i = \chi_m(x_i)$ along their diagonals.
- $U_\omega = \mathrm{diag}(\boldsymbol{u}_\omega) \in \mathbb{C}^{n\times n}$ is the diagonal matrix containing the vector $\boldsymbol{u}_\omega \in \mathbb{C}^n$ with the elements $[\boldsymbol{u}_\omega]_i = \hat{u}(x_i,\omega)$ along its diagonal.
- $\boldsymbol{u}_\omega^{\mathrm{in}} \in \mathbb{C}^n$ is the vector with the elements $[\boldsymbol{u}_\omega^{\mathrm{in}}]_i = \hat{u}(x_i,\omega)$.
- $\boldsymbol{r}_\omega \in \mathbb{C}^n$ is the vector with the elements $[\boldsymbol{r}_\omega]_i = hg(x_{\mathrm{r}} - x_i,\omega)$.
- $u_\omega^{\mathrm{sc}} \in \mathbb{C}$ is the complex number representing the scattered frequency-domain voltage $\hat{u}^{\mathrm{sc}}(x_{\mathrm{r}},\omega)$.

The numerical solution $\boldsymbol{u}_\omega$ of the forward scattering problem can be obtained by solving the linear algebraic problem (3.3). To solve the inverse scattering problem, one has to use both (3.3) and (3.4) to find the three vectors $\boldsymbol{x}_m$, $m = 1,2,3$.

3.2 Discrete Green's function of a homogeneous cable

There is a significant difference between the average power cable propagation constant γ and the vacuum propagation constant γ_0. The large jump in the propagation constant at the end of a finite cable produces the most noticeable (multiple) reflections of the electromagnetic wave propagating in the cable. The spatial variations of the constitutive parameters along the cable are relatively small compared to this jump.

Incorporating the reflections at the ends of the cable into the Green's function would have been beneficial for the inverse problem, as it would allow focusing on the relatively small spatial variations along the cable. However, computing the Green's function of a finite albeit homogeneous piece of cable, is a formidable task. In this section, we introduce the numerical analogue of this procedure.

Consider the following split of the contrast functions:

$$\begin{aligned}
\chi_1(x) &= R_{\mathrm{b}} G_{\mathrm{b}} + \tilde{R}(x)\tilde{G}(x) = \chi_1^{\mathrm{b}} + \tilde{\chi}_1(x), \\
\chi_2(x) &= R_{\mathrm{b}} C_{\mathrm{b}} + G_{\mathrm{b}}\mu_0 + \tilde{R}(x)\tilde{C}(x) + \tilde{G}(x)\mu_0 = \chi_2^{\mathrm{b}} + \tilde{\chi}_2(x), \\
\chi_3(x) &= \mu_0(\epsilon_0 - C_{\mathrm{b}}) + \mu_0(\epsilon_0 - \tilde{C}(x)) = \chi_3^{\mathrm{b}} + \tilde{\chi}_3,
\end{aligned} \tag{3.5}$$

where $\chi_m^{\mathrm{b}} \in \mathbb{R}$ are constants. The corresponding diagonal matrices will be split as follows: $X_m = \chi_m^{\mathrm{b}} I + \tilde{X}_m$, $m = 1, 2, 3$.

Introducing these representations in (3.3), we arrive at the problem:

$$[I - \chi_1^{\mathrm{b}} G_\omega - G_\omega \tilde{X}_1 - j\omega\chi_2^{\mathrm{b}} G_\omega - j\omega G_\omega \tilde{X}_2 - \omega^2 \chi_3^{\mathrm{b}} G_\omega - \omega^2 G_\omega \tilde{X}_3]\boldsymbol{u}_\omega = \boldsymbol{u}_\omega^{\mathrm{in}}, \tag{3.6}$$

which is equivalent to the problem:

$$[I - G_\omega^{\mathrm{b}} \tilde{X}_1 - j\omega G_\omega^{\mathrm{b}} \tilde{X}_2 - \omega^2 G_\omega^{\mathrm{b}} \tilde{X}_3]\boldsymbol{u}_\omega = \tilde{\boldsymbol{u}}_\omega^{\mathrm{in}}, \tag{3.7}$$

where

$$\begin{aligned}
G_\omega^{\mathrm{b}} &= [I - \chi_1^{\mathrm{b}} G_\omega - j\omega\chi_2^{\mathrm{b}} G_\omega - \omega^2 \chi_3^{\mathrm{b}} G_\omega]^{-1} G_\omega, \\
\tilde{\boldsymbol{u}}_\omega^{\mathrm{in}} &= [I - \chi_1^{\mathrm{b}} G_\omega - j\omega\chi_2^{\mathrm{b}} G_\omega - \omega^2 \chi_3^{\mathrm{b}} G_\omega]^{-1} \boldsymbol{u}_\omega^{\mathrm{in}}.
\end{aligned} \tag{3.8}$$

It is clear that G_ω^{b} is the discrete analogue of the Green's function of the homogeneous finite cable with the constitutive parameters given by the contrast functions χ_m^{b}, $m = 1, 2, 3$.

Chapter 4

Reconstruction of constitutive parameters

In this Chapter we propose a two-step procedure for reconstructing the constitutive parameters of the power cable. In the first step the effective parameters are reconstructed with a nonlinear optimization algorithm, using a spatially homogeneous model of the cable. In the second step a linearized method is applied to reconstruct the remaining spatial variations of the cable parameters.

4.1 Reconstruction of effective cable parameters

To reconstruct the effective background parameters one assumes that the constitutive parameters of a cable are homogeneous, i.e., the contrast functions are χ_m^{b}, $m = 1, 2, 3$. Then, the forward and inverse scattering problems become:

$$[I - (\chi_1^{\mathrm{b}} + j\omega\chi_2^{\mathrm{b}} + \omega^2\chi_3^{\mathrm{b}})G_\omega]\boldsymbol{u}_\omega^{\mathrm{b}} = \boldsymbol{u}_\omega^{\mathrm{in}}, \tag{4.1}$$

$$(\chi_1^{\mathrm{b}} + j\omega\chi_2^{\mathrm{b}} + \omega^2\chi_3^{\mathrm{b}})\boldsymbol{r}_\omega^T\boldsymbol{u}_\omega^{\mathrm{b}} = u_\omega^{\mathrm{sc}} \tag{4.2}$$

Solving (4.1) for $\boldsymbol{u}_\omega^{\mathrm{b}}$ and substituting the result in (4.2) we arrive at the equation:

$$(\chi_1^{\mathrm{b}} + j\omega\chi_2^{\mathrm{b}} + \omega^2\chi_3^{\mathrm{b}})\boldsymbol{r}_\omega^T[I - (\chi_1^{\mathrm{b}} + j\omega\chi_2^{\mathrm{b}} + \omega^2\chi_3^{\mathrm{b}})G_\omega]^{-1}\boldsymbol{u}_\omega^{\mathrm{in}} = u_\omega^{\mathrm{sc}}, \tag{4.3}$$

which explicitly defines the scattered frequency-domain voltage $u_\omega^{\mathrm{sc}}(\chi_1^{\mathrm{b}}, \chi_2^{\mathrm{b}}, \chi_3^{\mathrm{b}})$ as a function of the constitutive parameters of the cable.

Let $v_{\omega_p}^{\mathrm{sc}}$ be the scattered voltage measured at the location x_{r} at the frequencies ω_p, $p = 1, \ldots, P$; and $u_{\omega_p}^{\mathrm{sc}}(y_1, y_2, y_3)$ the scattered voltage calculated according to (4.3) with the substitutions $\chi_m^{\mathrm{b}} = y_m$, $m = 1, 2, 3$. Consider the following cost function:

$$f(y_1, y_2, y_3) = \sum_{p=1}^{P} \frac{\left| u_{\omega_p}^{\mathrm{sc}}(y_1, y_2, y_3) - v_{\omega_p}^{\mathrm{sc}} \right|^2}{\left| v_{\omega_p}^{\mathrm{sc}} \right|^2}. \tag{4.4}$$

The effective constitutive parameters of the cable can now be reconstructed by minimizing this function:

$$[\chi_1^{\mathrm{b}}, \chi_2^{\mathrm{b}}, \chi_3^{\mathrm{b}}] = \arg \min_{[y_1, y_2, y_3] \in \mathbb{R}^3} f(y_1, y_2, y_3). \tag{4.5}$$

4.2 Linearized reconstruction of cable inhomogeneities

Let the effective background parameters χ_m^{b} either known *a priori* or reconstructed using the optimization procedure described in the previous Section. Note that these parameters may

depend on the temperature of the cable. To reconstruct the remaining spatial variations of the contrast functions, both natural and induced by the temperature, we resort to the formulation involving the discrete background Green's function G_ω^{b}.

Let the temperature-induced spatial variations $\tilde{\chi}_m(x)$ relative to the background contrast χ_m^{b} be small. Then, one can apply the total voltage approximation in (3.7) by the total voltage in the effective homogeneous cable, namely, $\boldsymbol{u}_\omega \approx \tilde{\boldsymbol{u}}_\omega^{\mathrm{in}}$. Substituting this and the contrast splittings into the main equation of the inverse scattering problem (3.4), we arrive at the linearized problem:

$$\boldsymbol{r}_\omega^T \tilde{U}_\omega^{\mathrm{in}} \tilde{\boldsymbol{x}}_1 + j\omega \boldsymbol{r}_\omega^T \tilde{U}_\omega^{\mathrm{in}} \tilde{\boldsymbol{x}}_2 + \omega^2 \boldsymbol{r}_\omega^T \tilde{U}_\omega^{\mathrm{in}} \tilde{\boldsymbol{x}}_3 = \tilde{u}_\omega^{\mathrm{sc}}, \tag{4.6}$$

where

$$\tilde{U}_\omega^{\mathrm{in}} = \mathrm{diag}(\tilde{\boldsymbol{u}}_\omega^{\mathrm{in}}) = \mathrm{diag}\left([I - \chi_1^{\mathrm{b}} G_\omega - j\omega\chi_2^{\mathrm{b}} G_\omega - \omega^2 \chi_3^{\mathrm{b}} G_\omega]^{-1} \boldsymbol{u}_\omega^{\mathrm{in}}\right), \tag{4.7}$$

$$\tilde{u}_\omega^{\mathrm{sc}} = u_\omega^{\mathrm{sc}} - (\chi_1^{\mathrm{b}} + j\omega\chi_2^{\mathrm{b}} + \omega^2\chi_3^{\mathrm{b}}) \boldsymbol{r}_\omega^T \tilde{\boldsymbol{u}}_\omega^{\mathrm{in}}. \tag{4.8}$$

Notice that this linearization is better than the usual Born approximation where one assumes $\boldsymbol{u}_\omega \approx \boldsymbol{u}_\omega^{\mathrm{in}}$. First of all, $\tilde{\boldsymbol{u}}_\omega^{\mathrm{in}}$ represents a much better approximation of $\boldsymbol{u}_\omega$, since it includes the main multiple reflections from the cable ends. Secondly, the crucial contrast function splittings (3.5) guarantee the smallness of the perturbations $\tilde{\chi}_m$.

To recover the vectors of the contrast perturbations $\tilde{\boldsymbol{x}}_m$, $m = 1, 2, 3$, we shall utilize the scattered voltage data measured at x_{r} at the angular frequencies ω_p, $p = 1, \ldots, P$. To this end, we introduce the block-matrix formulation:

$$R\tilde{\boldsymbol{x}} = \tilde{\boldsymbol{u}}^{\mathrm{sc}}, \tag{4.9}$$

where the matrix $R \in \mathbb{C}^{P \times 3n}$ is given by

$$R = \begin{bmatrix} \boldsymbol{r}_{\omega_1}^T \tilde{U}_{\omega_1}^{\mathrm{in}} & j\omega_1 \boldsymbol{r}_{\omega_1}^T \tilde{U}_{\omega_1}^{\mathrm{in}} & \omega_1^2 \boldsymbol{r}_{\omega_1}^T \tilde{U}_{\omega_1}^{\mathrm{in}} \\ \boldsymbol{r}_{\omega_2}^T \tilde{U}_{\omega_2}^{\mathrm{in}} & j\omega_2 \boldsymbol{r}_{\omega_2}^T \tilde{U}_{\omega_2}^{\mathrm{in}} & \omega_1^2 \boldsymbol{r}_{\omega_2}^T \tilde{U}_{\omega_2}^{\mathrm{in}} \\ \vdots & \vdots & \vdots \\ \boldsymbol{r}_{\omega_P}^T \tilde{U}_{\omega_P}^{\mathrm{in}} & j\omega_P \boldsymbol{r}_{\omega_P}^T \tilde{U}_{\omega_P}^{\mathrm{in}} & \omega_P^2 \boldsymbol{r}_{\omega_P}^T \tilde{U}_{\omega_P}^{\mathrm{in}} \end{bmatrix}. \tag{4.10}$$

The right-hand side vector $\tilde{\boldsymbol{u}}^{\mathrm{sc}} = [\tilde{u}_{\omega_1}^{\mathrm{sc}}, \ldots, \tilde{u}_{\omega_P}^{\mathrm{sc}}]^T \in \mathbb{C}^P$ contains the modified scattered voltage multi-frequency data. The unknown vector $\tilde{\boldsymbol{x}} = [\tilde{\boldsymbol{x}}_1^T, \tilde{\boldsymbol{x}}_2^T, \tilde{\boldsymbol{x}}_3^T]^T \in \mathbb{R}^{3n}$ contains all three contrast perturbation vectors.

Since the scattered voltage data contain statistical noise, the problem is usually solved in the least-squared sense:

$$\tilde{\boldsymbol{x}}_{\mathrm{LS}} = \arg \min_{\tilde{\boldsymbol{x}} \in \mathbb{C}^{3n}} \|\tilde{\boldsymbol{v}}^{\mathrm{sc}} - R\tilde{\boldsymbol{x}}\|_2^2, \tag{4.11}$$

where the vector $\hat{\boldsymbol{v}}^{\mathrm{sc}} = [\tilde{v}_{\omega_1}^{\mathrm{sc}}, \ldots, \tilde{v}_{\omega_P}^{\mathrm{sc}}] \in \mathbb{C}^P$ contains the experimental version of the modified scattered voltage data $\tilde{\boldsymbol{u}}^{\mathrm{sc}}$ with

$$\tilde{v}_\omega^{\mathrm{sc}} = v_\omega^{\mathrm{sc}} - (\chi_1^{\mathrm{b}} + j\omega\chi_2^{\mathrm{b}} + \omega^2\chi_3^{\mathrm{b}}) \boldsymbol{r}_\omega^T [I - \chi_1^{\mathrm{b}} G_\omega - j\omega\chi_2^{\mathrm{b}} G_\omega - \omega^2 \chi_3^{\mathrm{b}} G_\omega]^{-1} \boldsymbol{u}_\omega^{\mathrm{in}}. \tag{4.12}$$

If the matrix $R^H R \in \mathbb{C}^{3n \times 3n}$, where R^H denotes the conjugate transpose of R, is invertible, then

$$\tilde{\boldsymbol{x}}_{\mathrm{LS}} = (R^H R)^{-1} R^H \tilde{\boldsymbol{v}}^{\mathrm{sc}}. \tag{4.13}$$

If the matrix $R^H R$ is not invertible, then the minimum-norm solution $\tilde{\boldsymbol{x}}^\dagger$ of the least-squares problem is computed as:

$$\tilde{\boldsymbol{x}}^\dagger = (R^H R)^\dagger R^H \tilde{\boldsymbol{v}}^{\mathrm{sc}}, \tag{4.14}$$

where $(R^H R)^\dagger$ denotes the generalized inverse of the matrix $R^H R$.

Chapter 5

Data pre-processing

In this Chapter, we perform the preliminary analysis of the reflectometry data obtained in the experiment carried out at Alliander B.V. We extract the incident and scattered signals in the time domain, perform their Fourier transforms, and arrive the quantities required by the frequency-domain formulation of the inverse scattering problem introduced in the previous Chapters.

5.1 Controlled-temperature experiment

In early 2023 Alliander conducted an experiment to establish the relation between temperature and propagation time for both XLPE and PILC cables. The purpose of the experiment was to properly establish how the propagation time changes as a function of the temperature in the entire range of temperatures experienced by a cable during operation. The goal was to confidently establish the nature of this relation for both XLPE and PILC cables.
The experiment was setup in the following way:

- A climate chamber was constructed to allow control over the temperature of the cable. (Figure 5.1a)
- A PILC and XLPE cable reel were placed inside the climate control chamber. (Figure 5.1b)
- SCG sensor units were placed at the beginning and end of the cable in order to measure the change in voltage over time. [6]
- Temperature sensors were placed on different locations of the cable reel.

After this initial setup the process of measuring propagation times at different temperatures can begin. In steps of 5°C between room temperature and 60°C the following steps were preformed.

1. Set heater to new temperature.
2. Wait 24 hours to allow the room and cable reel temperature to stabilize.
3. Measure the precise temperature.
4. Send a signal through the cable and measure the voltage.

In Figure 5.2 one of the measurements be seen in Figure 5.2. For $t \in [0, 2.5\mu s]$ the signal is sent, for $t \in [3.0\mu s, 5.0\mu s]$ the first reflection is measured, for $t \in [5.5\mu s, 7.0\mu s]$ the second reflection is measured, etc.

(a) Climate control chamber

(b) 415m of Telcon XLPE cable, 1x25mm^2 with Aluminum conductor and a $16mm^2$ cross section of the screen.

Figure 5.1: Setup of experiment performed in Duiven.

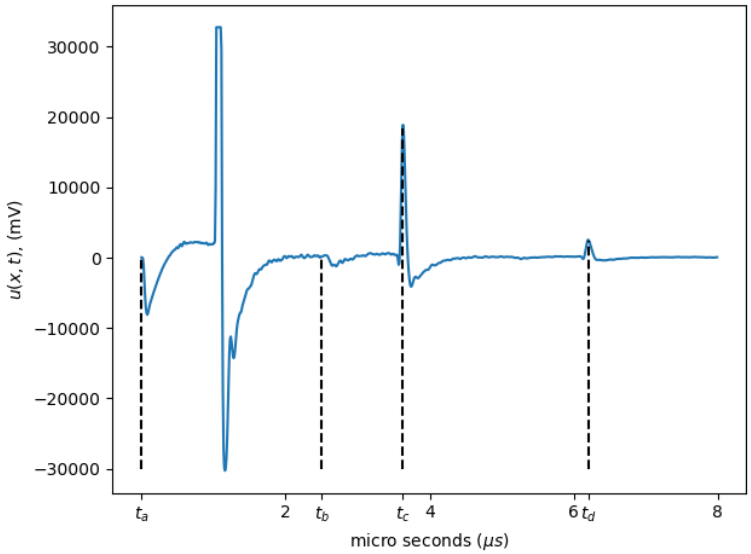

Figure 5.2: Measured voltage signal in the XLPE cable with $T = 19.4°C$.

5.2 Reconstruction of the truncated signal

In Figure 5.2, the detected signal $u(x,t)$ is shown. However, due to limitations of the measurement apparatus, the signal is not captured perfectly. Specifically, the measurement device does not record beyond certain limits, causing the signal to be truncated between $t \approx 1.0\mu$s and $t \approx 1.1\mu$s.

To reconstruct this peak we will make the following assumption. We expect the signal to reduce with the same factor after each reflection. To determine this factor, we will determine the factor by which the signal reduces between the first and second reflection, $t = t_c$ and $t = t_d$ respectively. These factors can be found in Table 5.1 per temperature. Multiplying the first reflection with this factor gives us the height of the original signal.

Next we we assume that our truncated signal is of the form $u(x,t) = a(x-p)^2 + q$. p lies in the center of our truncated signal, and q is equal to the height of our original signal found in Table 5.1. Finally we solve the formula for the truncated signal and reconstruct the peak. In figure Figure 5.3 the reconstructed peak can be found for $T = 19.4°$C.

temperature °C	first reflection (mV)	second reflection (mV)	factor	original signal (mV)
19.4	18332	2476	7.40388	135728
22	18920	2592	7.29938	138104
27.2	19944	2728	7.31085	145808
32.2	21004	2900	7.24276	152127
36	21584	2984	7.23324	156122
40.4	22496	3128	7.19182	161787
43.8	22288	3252	6.85363	152754
48.8	23164	3392	6.82901	158187

Table 5.1: For different temperatures the height of the first and second reflections, the factor between the first and second reflection and the reconstructed original height of the first signal.

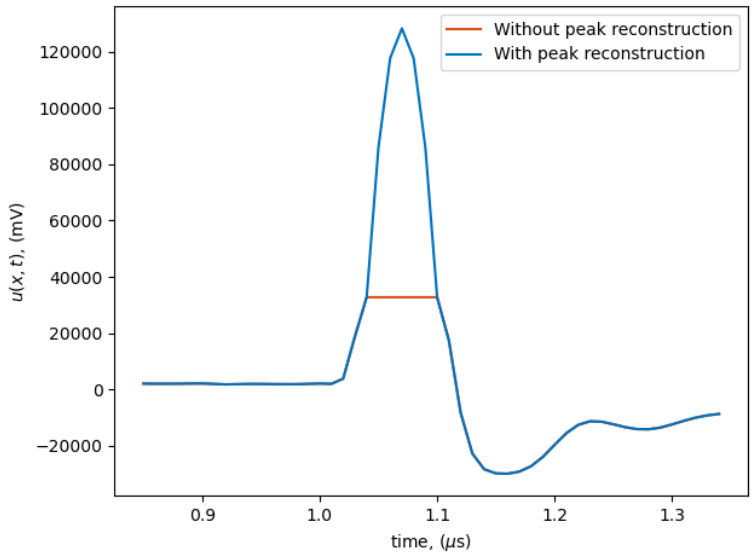

Figure 5.3: $u(x,t)$ with and without peak reconstruction.

5.3 Extracting the incident and scattered voltage data

In Figure 5.2 one can see the signal measured in the experiment at the temperature $T = 19.4°\mathrm{C}$. This signal is the total voltage data $U(x_\mathrm{r}, t)$ recorded at the receiver location x_r.

To arrive at the quantities used in the theoretical formulation of the previous Chapters, we first need to extract the incident and scattered voltages $U^\mathrm{in}(x_\mathrm{r}, t)$ and $U^\mathrm{in}(x_\mathrm{r}, t)$ in the time domain. Note that the additive property $U(x,t) = U^\mathrm{in}(x,t) + U^\mathrm{sc}(x,t)$ holds in the time domain as well. In particular, we have $U(x_\mathrm{r}, t) = U^\mathrm{in}(x_\mathrm{r}, t) + U^\mathrm{sc}(x_\mathrm{r}, t)$ at the receiver location.

Unfortunately, in this experiment, no separate measurement of $U^\mathrm{in}(x_\mathrm{r}, t)$ has been made. In fact, such a measurement is not too complicated, and is expected to be available in the future experiments. In the present case, we can still estimate $U^\mathrm{in}(x_\mathrm{r}, t)$ by exploiting the fact that the generated signal has a relatively short duration in time, whereas the significant length of the cable makes sure that the first reflections from its end are well-separated in time from the generator's signal recorded at the receiver location.

The vertical lines at t_a, and t_b in Figure 5.2 indicate the empirical boundaries of the incident voltage signal. Denoting by $U(x_\mathrm{r}, t)$ the measured total voltage signal, we define the approximate

$U^{\text{in}}(x_{\text{r}},t)$ and $U^{\text{sc}}(x_{\text{r}},t)$ as follows:

$$\begin{aligned} U^{\text{in}}(x_{\text{r}},t) &= \begin{cases} U(x_{\text{r}},t) & t\in[t_a,t_b] \\ 0 & t\notin[t_a,t_b] \end{cases} \\ U^{\text{sc}}(x_{\text{r}},t) &= U(x_{\text{r}},t)-U^{\text{in}}(x_{\text{r}},t). \end{aligned} \tag{5.1}$$

Denoting by $\mathcal{F}$ the Fourier transform, we subsequently compute:

$$\begin{aligned} \hat{u}^{\text{in}}(x_{\text{r}},\omega) &= \mathcal{F}[U^{\text{in}}(x_{\text{r}},t)] \\ \hat{u}^{\text{sc}}(x_{\text{r}},\omega) &= \mathcal{F}[U^{\text{sc}}(x_{\text{r}},t)] \end{aligned} \tag{5.2}$$

In Figure 5.4 $\hat{u}^{in}(x_R,\omega),\hat{u}^{sc}(x_R,\omega)$ can be found.

Extrapolating the incidental voltage along the cable

Finally, to arrive at the incident voltage that would have existed in the cable with the propagation constant γ_0, we assume that the source function $d\hat{f}/dx$ in the equation (2.7) is localized in space, namely:

$$\frac{d\hat{f}}{dx} = \hat{f}_0(\omega)\delta(x-x_{\text{r}}). \tag{5.3}$$

Applying the Green's Theorem we can express the solution $\hat{u}^{\text{in}}(x,\omega)$ of (2.7) as:

$$\begin{aligned} \hat{u}^{\text{in}}(x,\omega) &= \int_{\mathbb{R}} g(x-x',\omega)\frac{\hat{f}(x',\omega)}{dx'}\mathrm{d}x' \\ &= \int_{\mathbb{R}} g(x-x',\omega)\hat{f}_0(\omega)\delta(x_{\text{r}}-x')\mathrm{d}x' \\ &= g(x-x_{\text{r}},\omega)\hat{f}_0(\omega), \\ \hat{u}^{\text{in}}(x_{\text{r}},\omega) &= g(x_{\text{r}}-x_{\text{r}},\omega)\hat{f}_0(\omega) = -\frac{1}{2\gamma_0}\hat{f}_0(\omega), \\ \hat{f}_0(\omega) &= -2\gamma_0\hat{u}^{\text{in}}(x_{\text{r}},\omega), \\ \hat{u}^{\text{in}}(x,\omega) &= -2\gamma_0 g(x-x_{\text{r}},\omega)\hat{u}^{\text{in}}(x_{\text{r}},\omega). \end{aligned} \tag{5.4}$$

Upon substituting in the last formula above, the expression (2.12) for the Green's function, we arrive at:

$$\hat{u}^{\text{in}}(x,\omega) = \hat{u}^{\text{in}}(x_{\text{r}},\omega)e^{-\gamma_0|x-x_{\text{r}}|}. \tag{5.5}$$

Useful frequency band

In Figure 5.4 $\hat{u}^{in}(x_R,\omega)$ and $\hat{u}^{sc}(x_R,\omega)$ can be found. From this figure we can deduce that the interval $[0,4.0\times10^7]$ contains all the useful frequencies. Thus for the inverse scattering problem defined in the previous chapter we will use frequencies in this domain.

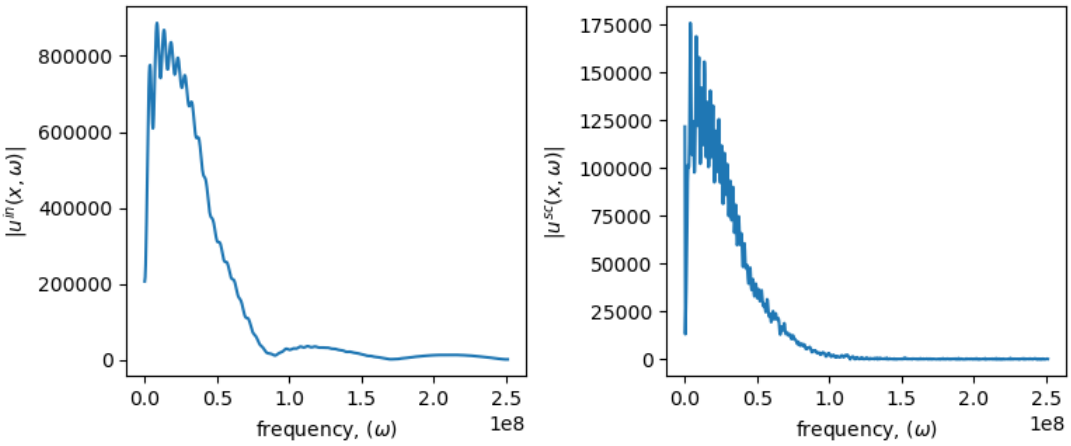

Figure 5.4: Incidental and scattered voltage in frequency domain.

Chapter 6

Numerical experiments with synthetic data

In the previous Chapter we defined the inverse scattering problem. In this Chapter, we implement the problem and test performance. We do this by creating synthetic data and testing our implementation on that.

6.1 Synthetic data

In order to test our data on synthetic data, we will first have to create our synthetic data. This is done in the following way. Our forward and inverse scattering problem is defined as in Equation (6.1) and Equation (6.2).

$$[I - (\chi_1^{\mathrm{b}} + j\omega\chi_2^{\mathrm{b}} + \omega^2\chi_3^{\mathrm{b}})G_\omega]\boldsymbol{u}_\omega^{\mathrm{b}} = \boldsymbol{u}_\omega^{\mathrm{in}}, \tag{6.1}$$

$$(\chi_1^{\mathrm{b}} + j\omega\chi_2^{\mathrm{b}} + \omega^2\chi_3^{\mathrm{b}})\boldsymbol{r}_\omega^T\boldsymbol{u}_\omega^{\mathrm{b}} = u_\omega^{\mathrm{sc}} \tag{6.2}$$

We will define most parameters as in Section 3.1 with 1 exception. Again we will have:

- $I \in \mathbb{R}^{n\times n}$ is the identity matrix.
- $G_\omega \in \mathbb{C}^{n\times n}$ is the matrix with the elements $[G_\omega]_{k,i} = hg(x_k - x_i, \omega)$.
- $X_m = \mathrm{diag}(\boldsymbol{x}_m) \in \mathbb{R}^{n\times n}$, $m = 1, 2, 3$, are the diagonal matrices that contain the vectors $\boldsymbol{x}_m \in \mathbb{R}^n$ with the elements $[\boldsymbol{x}_m]_i = \chi_m(x_i)$ along their diagonals.
- $U_\omega = \mathrm{diag}(\boldsymbol{u}_\omega) \in \mathbb{C}^{n\times n}$ is the diagonal matrix containing the vector $\boldsymbol{u}_\omega \in \mathbb{C}^n$ with the elements $[\boldsymbol{u}_\omega]_i = \hat{u}(x_i, \omega)$ along its diagonal.
- $\boldsymbol{u}_\omega^{\mathrm{in}} \in \mathbb{C}^n$ is the vector with the elements $[\boldsymbol{u}_\omega^{\mathrm{in}}]_i = \hat{u}(x_i, \omega)$ with $\hat{u}(x_i, \omega)$ as defined in Equation (5.5).
- $\boldsymbol{r}_\omega \in \mathbb{C}^n$ is the vector with the elements $[\boldsymbol{r}_\omega]_i = hg(x_{\mathrm{r}} - x_i, \omega)$.
- $u_\omega^{\mathrm{sc}} \in \mathbb{C}$ is the complex number representing the scattered frequency-domain voltage $\hat{u}^{\mathrm{sc}}(x_{\mathrm{r}}, \omega)$.

However, u_ω^{sc} will be created synthetically. To do this we will use typical values for R, G, C and L.

- To calculate the resistance R of our insulation material we will use the IEC classification of conductors [3]. For a aluminium insulator with a cross section of $25\,\mathrm{mm}^2$ $R \approx 1.20\,\Omega/\mathrm{km}$.

- The conductance of our insulation material G is expected to be very small as the electrical resistance of XLPE is very large. We let $G \in [10^{-25}, 10^{-5}]$.
- An approximation for the capacitance C is calculated using $C = 2\pi\epsilon_0\epsilon_r / \ln(D_{out}/D_{in})$ [4] where D_{in} is the diameter of the conductor material (5.64 mm) and D_{out} is the diameter of the insulation material and screen (7.13mm) and ϵ_r the relative permittivity of the insulation material (2.5) [5]. This gives $C \approx 5.93281306 \times 10^{-10}$. As this is an approximation we let $C \in [0.5 \times 5.93281306 \times 10^{-10}, 1.5 \times 5.93281306 \times 10^{-10}]$.
- In Section 2.5 we already defined $L = \mu_0$ as our cable is essentially non-magnetic.

Using these approximations for our constitutive parameters we can create u_ω^{sc} synthetically. Then we can test different minimization methods and analyse how well these methods perform in reconstructing our parameters.

6.2 Local minimisation

One way to find the minimum of our cost function Equation (4.4) is by using a local minimisation method. The Python package `scipy` offers various local minimization methods which all preform relatively the same. One of the local methods is the BFGS-B, a quasi-Newton method that is used for solving large-scale optimization problems with bound constraints on the variables.

To test whether the local minimization method accurately reconstructs our G and C we add some error to our initial guess x_0. If the reconstruction is accurate enough for small errors, we can apply the method to the real data. In figure Figure 6.1 the performance of the local optimization routine `scipy.optimize.minimize(cost_function, x0, method = BFGS-B, bounds)` is shown.

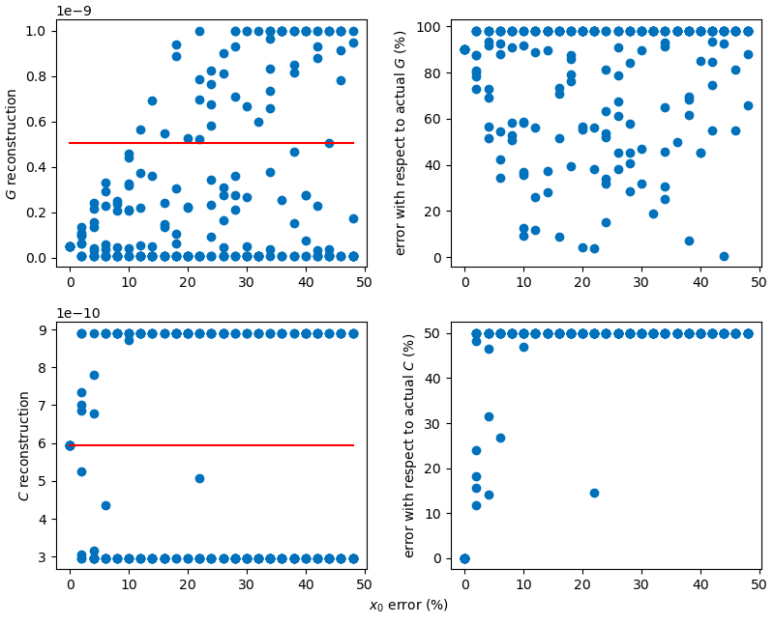

Figure 6.1: Performance of the `scipy.optimize.minimize(method = BFGS-B)` local optimization algorithm. The red horizontal line indicates the true solution. The blue dots correspond to reconstructions where the initial guess had an error corresponding to the x-axis

In the figure we can clearly see that even for extremely small perturbations of the initial guess x_0, the error on the reconstruction is extremely large: for only 10% error on x_0, the reconstructed C has more than 50% error with respect to the expected C. When applying our

implementation to the real data, we expect our initial guess to have an error of much more than 10%. This shows that the local optimisation algorithm is not accurate enough for our application.

6.3 Global optimisation with the Differential Evolution algorithm

As the available local optimisation method appears to be too sensitive with respect to the initial guess, we tested various global optimisation methods that generally do not have this problem. The method that produced the best results is the Differential Evolution (DE) algorithm. The DE method is stochastic in nature. It does not use the gradient of the cost functional to find its minimum, and can search large areas of the candidate space. At the same time, it often requires a significant number of iterations, i.e., function evaluations, compared to conventional gradient-based techniques.

Since the DE method is a global optimisation method, the bounds on variables need to be defined. We define the bounds using the realistic intervals of G and C found in Section 6.1. These are $[10^{-25}, 10^{-5}]$ and $[0.5 \times 5.93281306 \times 10^{-10}, 1.5 \times 5.93281306 \times 10^{-10}]$ respectively For the numerical experiments, we take random pairs of the values of G and C in these intervals and attempt their reconstruction. Figure 6.2a shows the results of these numerical experiments. Each line is the error in the reconstruction of one such set of randomly chosen parameters.

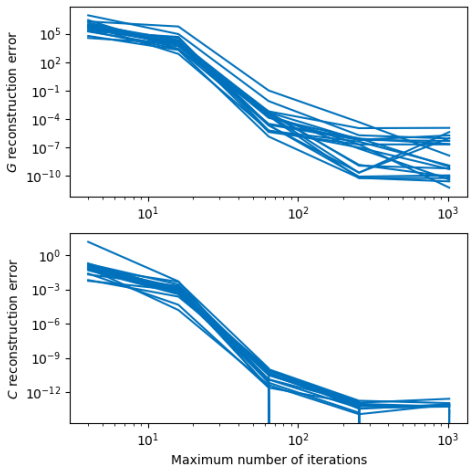

(a) Errors in the reconstruction of the synthetic G (top) and C (bottom) as functions of the number of iterations of the Differential Evolution algorithm

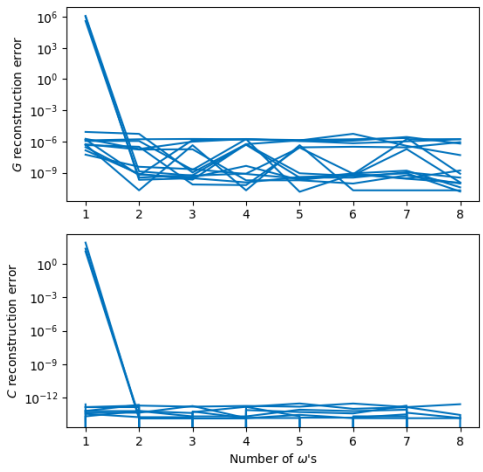

(b) Errors in the reconstruction of the synthetic G (top) and C (bottom) as functions of the number of frequency components used in the reconstruction process

Figure 6.2: Performance of the `scipy` Differential Evolution algorithm

The errors in the reconstruction of G and C tends to zero with the increasing number of iterations. On average we need 1024 iterations to find an acceptable solution.

One more aspect that can potentially affect the quality of the reconstruction is the number of frequency components, or simply frequencies ω, used in the cost functional. In Figure 6.2b G and C are reconstructed using an increasing number of frequencies. We evenly space our frequencies over the 'useful' interval $[0, 4 \times 10^7]$ that was established in Section 5.3. Again, each line is the reconstruction error for a single set of the randomly chosen G and C. We see that as long as we take multiple frequencies, the amount of frequencies is not as important for the accurate reconstruction of G and C.

Chapter 7

Application to measured data

In this Chapter, we apply the DE optimisation algorithm to the real data, reconstruct the constitutive parameters G and C at different temperatures and analyse the results.

7.1 Reconstruction of G and C

To recover the relation between the temperature and the parameters of the cable we reconstruct the constitutive parameters at each cable temperature individually, without assuming any *a priori* temperature dependence model.

Figure 7.1 shows the measured temperature over two days. As can be seen from this plot, the temperature of the cable is not consistent throughout the day, probably, due to the cyclic operation mode of the heater. Therefore, the reconstruction of constitutive parameters will be performed from several reflectometry measurements corresponding to the same nominal cable temperature. This will hopefully allow to average out the fluctuations in the temperature.

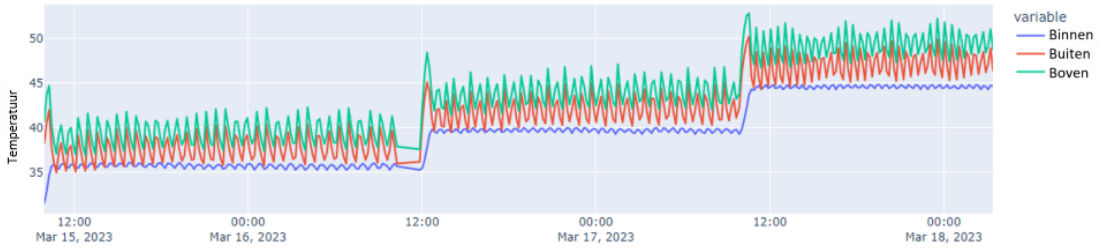

Figure 7.1: Temperature log of a part of the Duiven experiment

Figure 7.2 shows the reconstructed G and C at 8 different temperatures. Each dot corresponds to a reconstruction obtained from a single waveform measure by the reflectometer. At each temperature we observe a few outliers. Although, most of the reconstructions lie in a small interval.

The average conductivity G of the propagating medium (cable insulation layer) does not seem to depend on the cable temperature, while the average capacitance C of the insulating material decreases with temperature. This result is in agreement with the earlier conclusions in [2] that the propagation speed of the electromagnetic wave is increasing with the cable temperature in an XLPE power cable. This is further supported by the findings of Alliander that the propagation time of the electromagnetic wave is decreasing with an increasing cable temperature. The findings of Alliander can be found in Figure 7.3

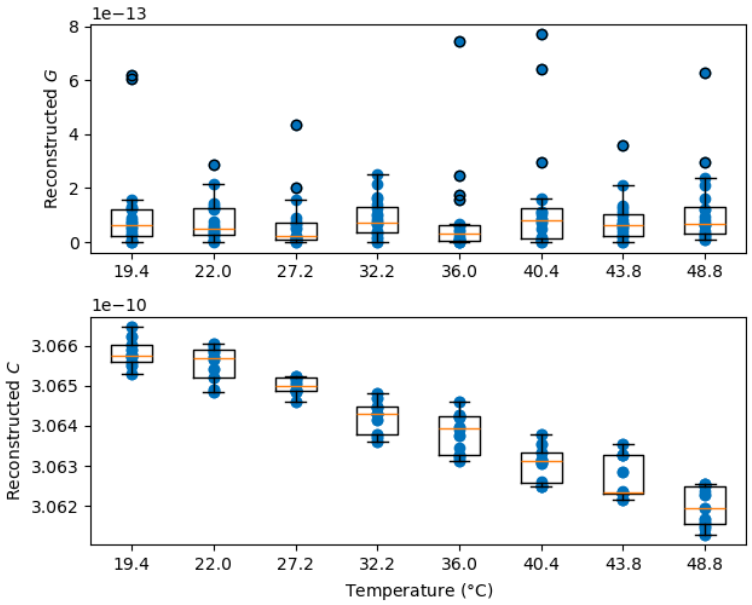

Figure 7.2: Reconstruction of G and C for a set of measurements per temperature. The box plot visualises the spread of the reconstruction per temperature.

7.2 Reconstruction of the temperature dependence

We fit a polynomial function $C_3(T)$ of the third degree in the temperature T to the median values of the reconstructed C. The resulting function is shown in Figure 7.4. The explicit expression for the fitted polynomial is:

$$C_3(T) = 1.23 \times 10^{-17} - 1.37 \times 10^{-15}T + 3.46 \times 10^{-14}T^2 + 3.06 \times 10^{-10}T^3 \tag{7.1}$$

It is obvious that this function is monotonically decreasing, which allows a unique recovery of the value of T, given the reconstructed value of C.

This temperature dependence may be different (e.g. increasing) for other cables (e.g. PILC) with a different type of insulating material. Therefore, a similar temperature-controlled experiment should be performed with each specific power cable and the corresponding temperature-dependence curves should be constructed.

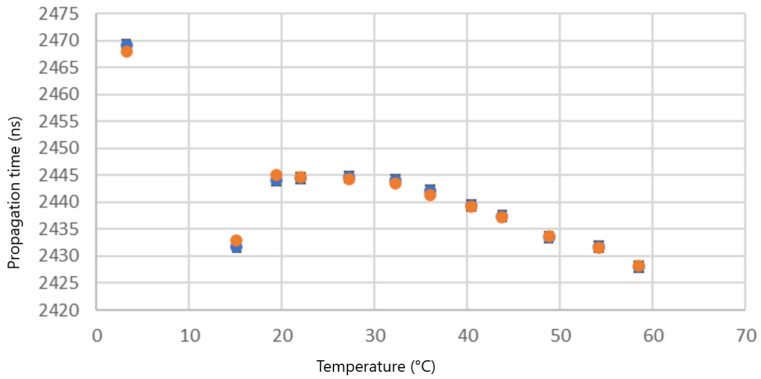

Figure 7.3: Propagation time of the electromagnetic signal sent through the XLPE cable. To note, the measurements below 20 degrees failed.

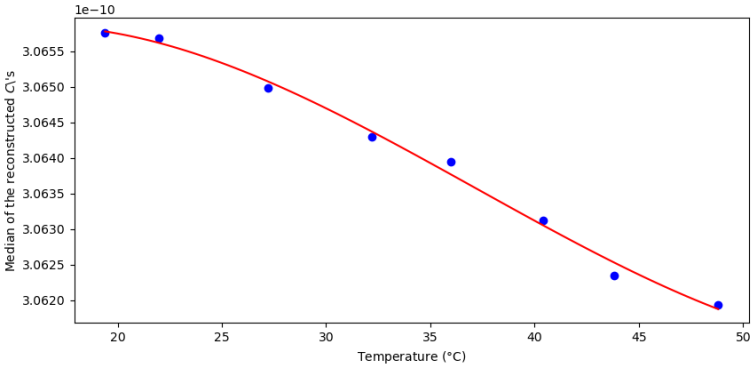

Figure 7.4: Fitted third degree polynomial to the median values of C as a function of T

Chapter 8

Conclusions

In this report an approach to the problem of the power-cable temperature reconstruction from the reflectometry data has been presented. The main idea of this project was to recover the electromagnetic constitutive parameters of the power cable and to analyze their dependence on the temperature from the data obtained during a temperature-controlled experiment. Knowing this parameter-temperature dependence, one can then apply the parameter-reconstruction algorithm and deduce the cable temperature in realistic conditions.

We have applied the Telegrapher's equations to model the propagation of the electromagnetic pulse in a power cable. We have further transformed the differential equations to the frequency domain, and applied the scattering formalism and the Green's Theorem to rewrite the problem of the reconstruction of the cable parameters as an inverse problem in the form of two coupled integral equations.

To take into account the finite length of the power cable, we have derived the discrete analogue of the finite-cable Green's function. A two-stage approach to the inverse scattering problem has been proposed, where in the first stage the effective homogeneous constitutive parameters of the cable are reconstructed without the usual linearizing approximation. Such a linearizing approximation is much more appropriate at the second stage, where the spatial inhomogeneities in the cable parameters are reconstructed.

In this report the first stage, i.e., the homogeneous-cable inverse problem, has been investigated in detail on both synthetic and experimental data. We have implemented the homogeneous cable model in python. We used Alliander's temperature-controlled experiment, where an approximate procedure for extracting the incidental and the scattered signals had to be applied, as only the total signal was measured.

We then tested the accuracy of our algorithm on synthetic data. The synthetic data was created by using the actual incidental signal and synthetic cable parameters. We investigated both local and global optimization algorithms and the global differential evolution (DE) algorithm showed the best performance.

Finally, we implemented the model on the temperature-controlled experiment of Alliander B.V. and reconstructed conductivity G and the capacitance C of the insulating material. The median of G showed no temperature dependence. The median of C showed a decreasing dependence on temperature for the XLPE power cable.

This temperature dependence of $C(T)$ has been fitted by a third degree polynomial. The dependence of C on T is monotonic. Hence, the cable temperature T of a homogeneous cable can be uniquely recovered from the reconstructed value of C.

While the results of this research are promising, several suggestions for the improvement of both the data-acquisition procedure and the reconstruction algorithm are in order. First of all, the approximate extraction of the incident signal should instead be implemented as a separate accurate measurement of the signal sent into the power cable. Secondly, the disappointing performance of the otherwise computationally efficient local gradient-based optimization algorithms can probably be improved by calculating the analytical gradient expression and supplying it to

the optimization routine. Finally, a separate experiment should be carried out to verify the ability of the present inversion method to reconstruct the spatial inhomogeneities of the power-cable temperature distribution.

Bibliography

[1] Wouters, P. A. A. F., van Deursen, A., & Li, Y. (2022). Analysis and verification of signal propagation as method for temperature monitoring of underground power cables. Electric Power Systems Research, 213, Article 108739. https://doi.org/10.1016/j.epsr.2022.108739

[2] Li, Y., Wouters, P. A. A. F., Wagenaars, P., Wielen, van der, P. C. J. M., and Steennis, E. F. (2013). Temperature dependency of wave propagation velocity in MV power cable. In 18th International Symposium on High Voltage Engineering (ISH 2013), August 25-30 2013, Seoul (pp. 1861-1866)

[3] Classification of conductors according to IEC 60228 https://www.google.com/url?sa=t&rct=j&q=&esrc=s&source=web&cd=&ved=2ahUKEwjtiaah5-KGAxXA9LsIHVdHCEQQFnoECE0QAQ&url=https%3A%2F%2Fwww.nexans.be%2Fen%2Fdam%2Fjcr%3Aefe5d9a2-f346-4047-87b4-99d1e319d768%2FIEC60228_ENG.pdf&usg=AOvVaw23ybd6_xdr0W4Hj-p1QZ9P&opi=89978449

[4] RATING OF ELECTRIC POWER CABLES; Ampacity Computations for Transmission, Distribution and Industrial Applications, George J. Anders, 1997

[5] Electric cables - Calculation of the current rating - Part 1: Current rating equations (100% load factor) and calculation of losses - General (IEC 60287-1-1: 2006, IDT)

[6] van der Wielen, P.C.J.M. (2005). On-line Detection and Location of Partial Discharges in Medium-Voltage Power Cables.

[7] Vuik, C., van Beek, P., Vermolen, F., van Kan, J., (2007). Numerical Methods for Ordinary Differential Equations

[8] Table of Fourier Transform Pairs https://uspas.fnal.gov/materials/11ODU/FourierTransformPairs.pdf

[9] Kress, C. (1999). Linear Integral Equations.